Title

Relationship Between Domain and Function of the Yeast RNase T2, Rny1p, Which Mediates rRNA Degradation upon Starvation

Author Affiliations

Atsushi Minami[1,*], Kohei Nishi[1,*], Rikusui Yamada[1,*], Gai Jinnai[1], Hikari Shima[1], Sakiko Oishi[1], Hirofumi Akagawa[1], Toshihiro Aono[2,4], Makoto Hidaka[1], Haruhiko Masaki[1], Tomohisa Kuzuyama[1,3], Yoichi Noda[1,3], and Tetsuhiro Ogawa[1,3]

[1]Department of Biotechnology, The University of Tokyo, Yayoi, Bunkyo-ku, Tokyo 113-8657, Japan.
[2]Agro-Biotechnology Research Center (AgTECH), The University of Tokyo, Yayoi, Bunkyo-ku, Tokyo 113-8657, Japan.
[3]Collaborative Research Institute for Innovative Microbiology (CRIIM), The University of Tokyo, Yayoi, Bunkyo-ku, Tokyo 113-8657, Japan.
[4]Present address: Institute for Agro-Environmental Sciences, National Agriculture and Food Research Organization. 3-1-3 Kannondai, Tsukuba, Ibaraki 305-8604, Japan.
[*]These authors contributed equally to this work.

Corresponding Author

Correspondence and requests for materials should be addressed to T.O. (email: atetsu@g.ecc.u-tokyo.ac.jp).

Running title

Mechanism of the stress response by yeast RNase T2

Abstract

RNase T2 is found in almost all organisms and non-living viruses. Although enzymatic activity is simple, RNase T2 involves diverse and essential roles in each species. *Saccharomyces cerevisiae* RNase T2, known as Rny1p, is localized in vacuoles and mediates rRNA degradation during autophagy of ribosomes. However, whether the ribosomal degradation is selective or non-selective or whether the two pathways coexist is still being determined. We found that most ribosomes are selectively degraded, and Rsa1p involves the degradation. As described, Rny1p is vacuolar-localized; however, some are secreted outside the cell and anchored to the host cell wall. Rny1p is characteristic of having a C-terminal extension with an unknown biological role. Our biochemical analyses indicated that the C-terminal extension is not required for the rRNA degradation but for anchoring Rny1p to the cell wall. Moreover, the predicted structure of the C-terminal extension of Rny1p superimposed well with sugar-binding domain-containing proteins, suggesting that Rny1p binds the sugar chain of the cell wall using the C-terminal extension. Phylogenetic analysis indicated that fungal RNase T2 evolved independently of RNase T2 from other species. Besides, structures of C-terminal extensions of other fungal RNase T2 proteins are almost identical to that of Rny1p. RNase T2 proteins from other than fungi also have C-terminal extensions. However, their sequences, structures, and biological functions differ from fungi. As the structures of the RNase domain of eukaryotic RNase T2 proteins are almost identical, the C-terminal extension confers species-specific functions to RNase T2.

Keywords
ribonuclease; ribosome; autophagy; structural model; molecular evolution

Introduction

RNA is an essential factor for life. It is an intermediate of the central dogma, connecting the genetic information encoded in DNA with the amino acid sequences of proteins. In addition, in recent years, considerable research has been conducted on RNAs that do not encode proteins but behave as functional molecules (1, 2). Other examples include RNAs that function as part of the immune system to eliminate foreign genes, such as by RNA interference (3, 4) and via the CRISPR system (5, 6). However, these RNAs have a lifespan and are eventually degraded. In addition, RNAs that are detrimental to life (e.g., owing to mutations) are actively degraded. Ribonucleases catalyze RNA degradation. There are two types of ribonucleases; an exonuclease type, which hydrolyzes RNA from the 5′ or 3′ ends, and an endonuclease type, which degrades phosphodiester bonds within the RNA molecule. Endonuclease-type ribonucleases are classified into three groups based on their structure, function, and base specificity (7). Among these, the RNase A family is the most well-known. Members of this family cleave single-stranded RNA and recognize pyrimidine bases. The other two groups are the RNase T1 and RNase T2 families. Like RNase A, these ribonucleases act on single-stranded RNA, with RNase T1 showing specificity for guanine and RNase T2 showing no apparent base specificity. These RNases use 2′,3′ cyclic monophosphates as intermediates upon cleavage, followed by forming a 3′ phosphate. Of these three families, RNase T2 is distinct from RNases A and T1 in two aspects. First, RNase A and RNase T1 show the highest enzymatic activities in the neutral pH range, whereas RNase T2 shows activity under acidic conditions. Second, RNase A is found in vertebrates, whereas RNase T1 is found in molds and bacteria. On the other hand, RNase T2 is present in almost all organisms whose genomes have been sequenced and in viruses. Thus far, it has not been reported in archaea or Gram-positive bacteria.

Although RNase T2 only has simple activity, as described above, it plays diverse and essential roles in each organism. For example, in humans, RNase T2 has been suggested to function as a cancer suppressor (8). Subsequently, deletions and mutations of the *RNASET2* gene have been reported in patients with congenital cystic leukoencephalopathy (9). Recently, a genome-wide association analysis has suggested that single nucleotide polymorphisms at the *RNASET2* locus are associated with multiple diseases (10–12). RNase T2 is also involved in innate immunity (13–16). In plants, RNase T2 is thought to be responsible for degrading extracellular nucleic acids and phosphate uptake in response to phosphate starvation (17–19). Additionally, in Solanaceae, Rosaceae, and Plantaginaceae, RNase T2, also known as S-RNase, is involved in self-incompatibility, which discriminates between self and non-self cells (20, 21). In viruses, RNase T2 attacks the immune cells of the infected host (22–24). Recently, it has been reported that, in *Escherichia coli*, 2′,3′-cyclic monophosphate nucleotides, which are intermediate products of RNA degradation by RNase T2, inhibit biofilm formation (25). Our research has aimed to uncover the fundamental principles that allow such functionally simple enzymes to play diverse and essential roles in various species.

RNase T2 is also present in budding yeast and is called Rny1p. This RNase is stress-responsive; e.g., Rny1p is required for growth at high temperatures and under high osmotic pressure (26). Rny1p enters the endoplasmic reticulum and is packaged into COPII vesicles. It is then transported to the Golgi apparatus and finally localizes to the vacuole, but some are secreted extracellularly and bind to the host cell wall (27). Also noteworthy is a functionally unknown C-terminal extension in Rny1p (Fig. 1A). However, the molecular mechanism whereby Rny1p responds to stress has been unknown. As RNase T2 targets ribosomal RNA (rRNA), a component of ribosomes (28–31), we hypothesized that Rny1p exhibits a stress response by degrading rRNAs. Therefore, we focused on a report describing ribosome degradation in response to rapamycin treatment in budding yeast (32). Rapamycin is an antibiotic that induces a nutrient starvation response in cells by inhibiting TOR (Target Of Rapamycin) complex 1, which plays a central role in nutrient source sensing.

Here, we provide novel insights into ribosomal degradation in response to nutrient starvation. Ribosome degradation involves autophagy, and Rny1p degrades rRNA in vacuoles, as previously reported (33). We revealed that most ribosomes are selectively degraded and that Rsa1p is required for the selectivity. This selective ribosomal degradation differs from the previously reported mechanism (34). Structural alignment and biochemical analyses revealed that Rny1p binds to the cell

wall via its C-terminal extension, independent of vacuolar rRNA degradation. The evolution of eukaryotic RNase T2 is discussed by comparing the C-terminal extension structure among the RNase T2 family.

Results

Rny1p is involved in various stress responses, including starvation

The *RNY1* promoter contains putative stress-responsive elements, and the PSY316 strain lacking Rny1p is sensitive to high temperatures and osmotic stress; however, these sensitivities were thought to be the PSY316 strain-specific (26). To verify this, a BY4742 strain (*MAT*α) was used instead. The BY4742 strain showed sensitivity to the above stresses. In addition to this, it was also sensitive to low temperature and oxidative stresses (Fig. 1B). Our experiments also indicated that Rny1p is responsible for stresses in haploid BY4741 (*MAT*a) and diploid BY4743 strains, respectively. These results indicate that the stress response by Rny1p is not unique to PSY316; however, BY4741 and BY4743 strains were less sensitive than the BY4742 strain to rapamycin (Fig. S1), suggesting differences in susceptibility among strains. For this reason, we decided to use BY4742 in this study.

As mentioned above, we focused on rapamycin-responsive rRNA degradation (32). Therefore, the sensitivity of the *rny1*Δ strain to rapamycin was evaluated first. The *rny1*Δ strain did not grow well on a solid medium containing 5 nM rapamycin, while the growth of the wild-type strain was not affected at all (Fig. 1C, left panel). To quantitatively analyze the effect of rapamycin on cell growth, wild-type and *rny1*Δ strains were grown in liquid medium containing rapamycin (100 nM). Under these conditions, the growth of the wild-type strain slowed down, but it continued during the experimental period. Cell growth was also delayed in the *rny1*Δ strain; however, it eventually ceased to grow (Fig. 1C, right panel).

Next, we evaluated rapamycin-induced rRNA degradation (Fig. 2A). In the wild-type strain, 18S and 25S rRNAs were degraded by adding 100 nM rapamycin. rRNA degradation was also observed in the *rny1*Δ strain; however, it occurred slower. The bands corresponding to the 35S precursor rRNA became faint after 1 h of rapamycin addition in both the wild-type and *rny1*Δ strains, indicating that rRNA synthesis was promptly impaired (35). To assess the degree of rRNA degradation in more detail, we calculated the ratio of rRNA remaining after rapamycin treatment using quantitative RT-PCR (qRT-PCR) (Fig. 2B). After the addition of rapamycin, 18S and 25S rRNA levels decreased to approximately 10% of those in wild-type cells. In comparison, about 35% and 25% of 18S and 25S rRNA remained in *rny1*Δ cells. 25S rRNA was more degraded than 18S rRNA in both the wild-type and *rny1*Δ strains, suggesting that 25S rRNA was more sensitive to Rny1p than 18S rRNA. The 35S rRNA level decreased to below 10% after rapamycin treatment, which is consistent with the results shown in Fig. 2A and those of previous studies (35).

Autophagic activity is decreased in *rny1*Δ cells

While our study is in progress, Huang *et al*. reported that nitrogen starvation induces ribosomal degradation and that Rny1p is required for the first step of the degradation process (33). They also showed that RNA accumulates in the vacuoles of *rny1*Δ cells under nitrogen starvation by fluorescence microscopic analysis (33). We observed the same phenomenon in rapamycin-treated *rny1*Δ cells (Fig. S2). Hereafter, nitrogen starvation was used instead of rapamycin treatment.

In *Arabidopsis*, RNase T2 (RNS2) depletion increases autophagosome (36). This result suggests that rRNA accumulation affects autophagic activity in yeast as well. We tested this hypothesis by performing a green fluorescent protein (GFP) cleavage assay. GFP-Atg8p was expressed in wild-type, *rny1*Δ, and *atg2*Δ strains, and nitrogen starvation was induced. The autophagic activity was evaluated based on the detection of GFP fragments by western blotting. Almost all the GFP-Atg8p was cleaved to GFP fragment after 6 h of starvation in the wild-type strain, while approximately half of the GFP-Atg8p remained intact in the *rny1*Δ strain (Fig. 3A). Moreover, continued nitrogen starvation appeared to increase GFP-Atg8p levels in *rny1*Δ cells, which was also observed by fluorescence microscopic analysis (Fig. S3). However, the fluorescence intensity of GFP in the vacuole was low in many *rny1*Δ cells compared to wild-type cells (Fig. S3), suggesting that autophagosomes do not fuse well with vacuoles in *rny1*Δ cells. To quantify the autophagic activity of wild-type and *rny1*Δ cells under nitrogen starvation, we performed the alkaline phosphatase (ALP)

activity assay. This assay revealed that ALP activity was lower in *rny1*Δ cells than in wild-type cells (Fig. 3B). Together, the impairment of Rny1p-mediated rRNA degradation reduces autophagic activity, as shown in *Arabidopsis*.

Rsa1p is involved in ribosome-specific degradation

Kraft *et al*. reported that ribosomes are degraded by a selective autophagy process termed "ribophagy" under nitrogen starvation (34). However, the receptor for specific ribosomal degradation has not yet been identified. On the other hand, some ribosomes are also degraded by non-selective autophagy under the same conditions (33). Therefore, whether ribosomal degradation is selective or non-selective, or whether the two types coexist is unclear. Recently, it was reported that, upon mTOR inactivation, ribosomes bind to nuclear fragile X mental retardation–interacting protein 1 (NUFIP1) and are delivered to autophagosomes for selective degradation in mammalian cells (37). We hypothesized that Rsa1p, a functional homolog of NUFIP1 in *S. cerevisiae*, is involved in selective ribosome degradation, together with Rny1p. Rsa1p serves as a platform for box C/D small nucleolar ribonucleoprotein (snoRNP) assembly (38–40) as well as NUFIP1 and localizes to the nucleus. First, to determine whether the degradation of ribosomal proteins depends on Rsa1p, we induced nitrogen starvation in cells expressing ribosomal protein L25 fused with GFP (Rpl25p-GFP) from the chromosome and performed a GFP cleavage assay (Fig. 4A). The number of GFP fragments increased in wild-type cells over time. In contrast, the fragment was barely detectable in *rsa1*Δ cells; a faint band was observed after 6 h of nitrogen starvation. We next investigated the involvement of Rsa1p in rRNA degradation using fluorescence microscopy (Fig. 4B). In *rsa1*Δ cells, RNA accumulation in the vacuoles was not observed. After 3 h of nitrogen starvation, RNA accumulation was slightly observed in *rsa1*Δ*rny1*Δ cells. We further quantified RNA degradation in each cell type using qRT-PCR (Fig. 4C). Although *RNY1* was intact, RNA was more abundant after starvation in *rsa1*Δ cells than in wild-type cells. This result indicated that rRNA degradation depends on Rsa1p, which is consistent with the results shown in Fig. 4B. The results shown in Figs. 4A, B, and C demonstrate that a Rsa1p-dependent selective ribosomal degradation pathway indeed exists. As ALP and GFP cleavage assays indicated that autophagic activity was almost comparable in *rsa1*Δ and wild-type cells after the induction of starvation (Figs. 4D and S4), we concluded that Rsa1p does not perturb non-selective autophagy.

Rny1p is anchored to the cell wall via its C-terminal extension, which is not required for ribosome degradation in the vacuole

As shown in Fig. 1A, Rny1p possesses the C-terminal extension with an unknown function. To investigate whether the C-terminal extension is required for rRNA degradation, we replaced genomic *RNY1* with *RNY1-F*, *RNY1ΔC-F*, or *RNY1(H87F/H160F)-F*, and induced nitrogen starvation in the resultant strains expressing Rny1p-F, Rny1pΔC-F, or Rny1p (H87F/H160F)-F, respectively (see Experimental procedures). Vacuolar RNA accumulation was observed in *rny1*Δ and Rny1p (H87F/H160F)-F-expressing strains under a fluorescence microscope (Fig. 5A). On the other hand, RNA accumulation was not observed in the strain expressing Rny1p-F or Rny1pΔC-F, indicating that the C-terminal extension is dispensable for RNA degradation in the vacuole.

As mentioned, Rny1p is localized in the vacuole, whereas some Rny1p is secreted outside and anchored to the host cell walls (27). However, the mode of cell wall anchoring, and its biological roles remain unclear. As the C-terminal extension is not involved in RNA degradation (Fig. 5A), we assumed that the extension is required for the cell wall anchoring. First, we performed a similarity search for the amino acid sequence of the C-terminal extension using Protein BLAST to elucidate the mechanism. However, no homologous proteins, other than RNase T2, were identified. Additionally, HMMer, a domain motif search method that uses a hidden Markov model, did not detect any known domain motifs. Therefore, we failed to estimate its function based on its sequence. We then attempted to elucidate the role of the C-terminal extension from a structural perspective. We predicted the overall structure of Rny1p using AlphaFold2 (41) (Fig. 5B). According to the predicted structure, the C-terminal extension of Rny1p was distinguishable from the structure of the RNase domain. Next,

we searched for similar protein structures on the Dali server (42) using the predicted structure of the C-terminal extension as a query. The top five structures are summarized in Table S2. Interestingly, they are all known or suggested to contain domains involved in sugar binding. We superimposed the C-terminal extension of Rny1p onto HA-33 (PDB ID:5B2H) (43), which has the highest Z-score (Fig. 5C). The predicted structure of the C-terminal extension of Rny1p and the structure of the variable region of HA-33 are similar despite the low amino acid sequence similarity between them. HA-33 forms a trimer complex with HA-17, which is involved in transporting a large toxin complex produced by *Clostridium botulinum* across the intestinal epithelial cell layer, and HA-33 binds the sugar chain on the cell surface. These structural analyses suggest that the C-terminal extension of Rny1p and the variable region of HA-33 share the same function.

The structural similarity of the C-terminal extension of Rny1p to sugar-binding domain-containing proteins suggests that Rny1p binds to the sugar chain of the cell wall via the C-terminal extension. Due to the low intracellular level of Rny1pΔC, we cloned each of the genes encoding C-terminally FLAG-tagged wild-type Rny1p (Rny1p-F) or that lacking the C-terminal extension (Rny1pΔC-F) in a high-copy plasmid and introduced each of them to the wild-type strain. We then cultured the resultant strains, prepared cell lysates from the cultured strains, and performed western blotting. Simultaneously, we collected the cultured medium, concentrated by ultracentrifugation, and electrophoresed with the cell lysate. Smeared bands were observed in the lane where the Rny1pΔC-F cultured concentrated medium was loaded (Fig. S5A). This suggested that Rny1pΔC-F is secreted and released into the medium. To analyze this further, we prepared cell lysates and cultured media, as shown in Fig. S5, and used endoglycosidase H (Endo H) to eliminate glycosylation (Fig. 5D, upper panel). Endo H treatment to cell lysate converted to a single band of Rny1p-F, which migrated in the original molecular weight position, indicating that Rny1p-F is glycosylated, as previously reported (27). A smeared band was also detected in the lysate of cells expressing Rny1pΔC-F, indicating that the lack of the C-terminal extension did not impair glycosylation. Moreover, as expected, Rny1pΔC-F was remarkably detected in the Endo-H-treated medium, while Rny1p-F was not detected (Fig. 5D, upper panel). We performed the same experiment using samples prepared under nitrogen starvation condition (Fig. 5D, bottom panel). The band signal for Rny1pΔC-F prepared from the medium was slightly weaker than that prepared from the cell lysate, suggesting that the trafficking of Rny1p is changed upon starvation. We also verified that the band signal of secreted Rny1pΔC-F, treated with Endo H, became weaker in the nitrogen-depletion condition than in the nitrogen-containing condition by western blotting on the same membrane (Fig. S5B). Moreover, we prepared spheroplasts from cells with or without a nitrogen source to separate the cytosolic and cell wall fractions and performed SDS-PAGE and western blotting analysis, as shown in Fig. 5D. These analyses demonstrated that Rny1p-F levels in the cell wall fraction were significantly reduced in response to nitrogen starvation. In contrast, no apparent changes in intracellular Rny1p-F levels were observed (Fig. 5E).

Diversity and the roles of the C-terminal extension of the RNase T2 superfamily

To investigate the conservation of the C-terminal extension among RNase T2 family members, we performed a molecular phylogenetic analysis based on RNase T2 sequences, with annotations reviewed in Swiss-Prot. The overall sequence similarity is low because RNase T2 is defined by only two conserved active sites (CASI and CASII). Therefore, we thought phylogenetic analysis based on the usual multiple alignments was unsuitable. Instead, we used the Graph Splitting method (44) to reconstruct a phylogenetic tree containing the remote homologs. The phylogenetic analysis showed that fungal RNase T2 diverged from the other RNase T2 proteins at an early stage in the phylogenetic tree, suggesting that they evolved independently (Fig. 6A). A portion of fungal RNase T2, labeled in yellow in the phylogenetic tree, has a long domain exceeding 100 amino acids at the C-terminus (Fig. S6A). Among them, RNase T2 proteins, termed Le37 and Irp3, from *Lentinus edodes* and *Irpex lacteus*, respectively, have low amino acid sequence similarity to Rny1p; however, they share some critical amino acid residues (45), suggesting that their C-terminal extensions of RNase T2 have a similar role to that of Rny1p. Since Le37 and Irp3 are homologous, we selected Irp3 and predicted its structure using AlphaFold2 (Fig. S6B). The predicted structure of the C-terminal extension of Irp3

is compared well with that of Rny1p, with a root mean square deviation (RMSD) of 2.91 Å, which is lower than that of HA-33 (Fig. 6B). Moreover, the predicted structures of C-terminal extensions of other fungal RNase T2 proteins (shown in Fig. 6A, shaded in yellow) are almost the same as the structure of that of Rny1p (Fig. S6C and D).

In contrast, some RNase T2 proteins, other than those in fungi, also have C-terminal extensions, but their sequences and structures are different from that of Rny1p. For example, E^{rns}, a glycoprotein produced by the classical swine fever (CAF) virus, contains a motif characteristic of RNase T2 and exerts RNase activity (22, 46). E^{rns} also has a C-terminal extension that is required for receptor-independent translocation across the cell membrane (47). According to the prediction by AlphaFold2, the C-terminal extension of E^{rns} forms an α-helix structure ((Fig. S6E), which is quite different from that of Rny1p. Other examples include the C-terminal extension of the class II plant RNase T2, which is necessary for localization to the vacuole (48), and *Caenorhabditis elegans* RNase T2 (49). Their C-terminal extensions are shorter than that of Rny1p and may have evolved independently, based on the phylogenetic tree (Fig. 6A). We attempted but failed to predict the structure of these C-terminal extensions; they seemed disordered. Based on these analyses, the diversity of the C-terminal extension may result from the evolution of the RNase T2 family, depending on where they function in each organism.

Discussion

We showed that Rny1p responds to various stresses, including starvation, as shown in Fig. 1B and C. Furthermore, our findings indicate that most, if not all, ribosomes are selectively degraded in response to nitrogen starvation. This selective ribosomal degradation seems to differ from the process previously reported for ribophagy, as its factors, such as Ubp3, Ufd3p, and Cdc48p (34, 50), are unnecessary (Fig. S7). Selective autophagy requires a receptor specific to the degradation target, and our study indicates that Rsa1p plays this role in yeast. Impairment of ribosome-specific degradation did not influence bulk autophagy, indicating that selective ribosome degradation does not compete with bulk autophagy (Fig. 4D). NUFIP1, the mammalian homolog of Rsa1p, forms a complex with the small protein ZNHIT3 (zinc finger HIT domain-containing protein 3) and is involved in the assembly of box C/D snoRNP, as described above. NUFIP1 localizes primarily in the nucleus, but is also present in the cytoplasm of certain cell types (51). The inhibition of mTORC1, a mammalian homolog of yeast TORC1, by starvation or the addition of its inhibitors results in the localization of the NUFIP1-ZNHIT3 complex from the nucleus to autophagosomes and lysosomes. NUFIP1 also binds to ribosomes and LC3B, an ortholog of the yeast protein Atg8p. The depletion of NUFIP1 prevents the autophagic degradation of ribosomes, indicating that NUFIP1 is a receptor for the selective autophagy of ribosomes in mammalian cells (37). It has been reported that Hit1p is an interacting partner of Rsa1p and is cooperatively involved in box C/D snoRNP assembly (52). Therefore, Rsa1p and Hit1p may form ribosomal receptors in yeast. When cells are exposed to stresses, such as starvation, new ribosome synthesis and the initiation step of protein synthesis are inhibited. However, some ribosomes should synthesize proteins required for adaptation to stress conditions. Therefore, the nonspecific engulfment of cytoplasmic ribosomes by autophagosomes appears to be inefficient. Because NUFIP1 and Rsa1p are involved in ribosome biosynthesis in the nucleus, it is possible that the ribosomes to be selectively degraded are not those in the cytoplasm but those in the composition process in the nucleus. Under stress conditions, incomplete ribosomes in the nucleus are unnecessary; therefore, they are likely targets of selective degradation. If this is correct, the selective degradation of ribosomes shown here does not interfere with ribosomes attempting to translate stress response factors in the cytoplasm.

GFP cleavage and ALP assays showed that the *rny1*Δ strain decreases bulk autophagy activity, indicating that the impairment of RNA degradation in vacuoles is harmful to cells, which may result in the growth defect in the stress condition. Additionally, Atg8p synthesis was upregulated in the *rny1*Δ strain upon starvation (Fig. 3), suggesting that cells increase the expression levels of Atg8p to facilitate autophagic degradation of RNA in the vacuole. As mentioned above, after the induction of nitrogen starvation, wild-type and *rny1*Δ strains expressing GFP-Atg8p were observed by fluorescence microscopy (Fig. S3). Fewer cells showed GFP signals in the vacuoles in the *rny1*Δ strain than in the wild-type strain. This suggests that autophagosome fusion with vacuoles is reduced in *rny1*Δ cells. The reason is likely due to the accumulation of undegraded RNA in the vacuoles of *rny1*Δ cells; however, the details of the mechanism could not be clarified in this study.

After glycosylation, Rny1p is transported to the vacuole, whereas some Rny1p is secreted out of the cell and anchored to the host cell wall (27). Although the C-terminal extension of Rny1p has no homologous sequence other than RNase T2, its structure resembles that of a sugar-binding domain, suggesting that Rny1p anchors to the sugar chain of the cell wall via the C-terminal extension. Based on this suggestion, we successfully revealed that cell wall anchoring of Rny1p requires the C-terminal extension of Rny1p. Moreover, cell wall anchored Rny1p is unnecessary for rRNA degradation in vacuoles. However, the mechanism by which Rny1p is differentially transported into the vacuole and extracellular space remains unknown. After nitrogen starvation was induced, the amount of extracellular Rny1p decreased (Fig. 5D, E, and S5B), suggesting that starvation changes the cellular trafficking of Rny1p.

Although the physiological role of cell wall anchoring is unknown, one possible role is the degradation of extracellular nucleic acids for their uptake as nutrients. An example of a similar function is tomato RNase T2 (RNase LE), which is secreted during phosphate starvation and degrades extracellular RNA (53). This study indicated that at least the C-terminal extension is required for

growth at high temperatures (Fig. S8). Yeast has a signaling pathway known as the cell wall integrity (CWI) pathway, which is activated by heat stress to alter the structural state of the cell wall (54). Thus, cell wall anchored Rny1p may be involved in regulating CWI. The most attractive idea is that some extracellular RNAs bind to cell membranes to regulate their ion permeability (55), and Rny1p degrades these RNAs for regulation. Further studies are required to clarify the function of the C-terminal extension of Rny1p.

The C-terminal extensions of fungal RNase T2 proteins, including Irp3 produced by *Irpex lacteus*, were predicted to have almost the same structure as that of Rny1p. In contrast, the C-terminal extension of E^{rns}, which is required to across cellular membranes in a receptor-independent manner, had a different structure (Fig. 6B and S6E). The Graph Splitting method suggested that fungal RNase T2 evolved independently from animal and plant RNase T2 (Fig. 6A). In contrast, the X-ray crystal structures of *Pyrus pyrifolia* and *Homo sapiens* RNase T2 were well superposed on the predicted structure of the RNase domain of Rny1p (Fig. S9). The presence of RNase T2 in almost all organisms suggests that cells have retained RNase T2 since the early stage of evolution. Over its long evolutionary history, it has come to play a specific role in many species. Acquisition of the C-terminal extension is one of the reasons why such enzymatically simple ribonucleases have taken on diverse roles in different species. To better understand this process, it is necessary to clarify the structure and function of the C-terminal extension of the RNase T2 family.

Experimental procedures

Yeast strains, plasmids, and culture conditions

The strains used in this study are listed in Table 1. The pRS316[GFP-ATG8] plasmid expressing Atg8p fused with GFP at the N-terminus was provided by the National Bio-Resource Project (NBRP) – Yeast, Japan. The strain genetically expressing Rpl25p-GFP (56) was gifted by Professor Hiroshi Takagi. The pGMH20 was provided by the RIKEN BRC through the National Bio-Resource Project of the MEXT, Japan (cat. RDB01956). The strains were cultured in YPD (1% yeast extract, 2% polypeptone, 2% glucose) or synthetic dextrose (SD) medium (0.67% nitrogen base without amino acids, 2% glucose) at 30°C. For gene expression under the control of the *GAL1* promoter, cells were cultivated overnight in a synthetic medium containing raffinose instead of glucose (SRaf medium). After the cells were washed, they were inoculated into synthetic galactose (SG) medium to achieve an OD_{660} of 0.1, and cultivation was re-initiated. Rapamycin was used at a final concentration of 100 nM to induce cell starvation. Nitrogen-depleted (SD (-N)) medium containing 0.17% yeast nitrogen base without amino acids and ammonium sulfate, and 2% glucose was used to induce nitrogen starvation.

Reagents

Rapamycin (a mixture of isomers) was purchased from FUJIFILM Wako Pure Chemical Corporation and dissolved in DMSO. LongLife Zymolyase was purchased from G-Bioscience. Endoglycosidase H (Endo H) was purchased from New England Biolabs.

Plasmid construction

Genes for wild-type Rny1p and those lacking the C-terminal extension (Rny1pΔC) without stop codons were PCR amplified to introduce *Eco*RI and *Xho*I sites at the 5′ and 3′ ends, respectively. They were then digested with *Eco*RI and *Xho*I and inserted into the same restriction sites of pYN735 to yield fusion genes with a 3xFLAG tag coding region at the 3′ ends. These genes were excised with *Eco*RI and *Sal*I, and inserted into the same restriction sites of pGMH20, a high-copy number plasmid containing the *GAL1* promoter and *HIS3* marker. The resultant plasmids, pGMH20-*RNY1-F* and pGMH20-*RNY1*ΔC-*F*, express Rny1p and Rny1p lacking the C-terminal extension, respectively, with 3xFLAG-tag fused at each of their C-termini. A plasmid expressing catalytically inactive Rny1p was prepared to introduce mutations to exchange the 87th and 160th histidine residues with phenylalanine using the QuickChange site-directed mutagenesis method, and the plasmid was designated pGMH20-*RNY1(H87F/H160F)-F*. These plasmids were introduced into BY4742 background strains, and these genes were expressed under the control of the *GAL1* promoter.

Strain construction

Wild-type *RNY1* and *HIS3* cassettes were PCR amplified to introduce homologous regions of 5′ and 3′ sides of genomic *RNY1* to the amplified fragment of both ends using pGMH20-*RNY1-F* as a template. The amplified fragment was transduced into the BY4742 strain, and the genomic *RNY1* gene was replaced by double-crossover homologous recombination. Transformants were plated onto SD medium containing leucine, lysine, and uracil at 30°C and incubated until visible colonies were obtained. Transformants in which the native *RNY1* gene was successfully replaced with the transduced gene were screened using colony PCR. Similarly, DNA fragments containing genes encoding Rny1pΔC or Rny1p (H87F/H160F) and the *HIS3* cassette were amplified from pGMH20-*RNY1*ΔC-*F* or pGMH20-*RNY1(H87F/H160F)-F* as described above and integrated into the genome. The *HIS3* cassette was replaced with the *RNY1* gene to construct the *rny1*Δ strain, which is used as a control. The *RNY1* gene of these transformants was amplified using PCR and sequenced to determine whether the transduced fragments were adequately integrated.

Measurement of cell growth

Cells were grown in a YPD medium at 30°C until the optical density at 660 nm (OD_{660})

reached 0.3–0.4. These cultures were serially diluted five times; spotted on plates containing 50 g/L NaCl, 0.3 mM H_2O_2, and 5 nM rapamycin; and cultivated at 30°C until visible colonies were formed. To analyze sensitivity to heat shock, the plates were incubated at 39°C. To evaluate cold-shock sensitivity, the plates were incubated at 4°C for 2 days, followed by further incubation at 30°C for 1 day. To assess the effect of starvation on cell growth over time, the wild-type and *rny1*Δ strains were grown in a liquid YPD medium until the OD_{660} reached 0.4. Then 100 nM rapamycin was added, and cell growth was monitored using an OD-Monitor & T instrument (TAITEC). In all experiments concerning rapamycin treatment, DMSO was used as the solvent for rapamycin and was added as a mock treatment. We confirmed that DMSO did not affect the growth of the strains used here. To examine the extent of RNA degradation in cells cultured in YPD, the OD_{660} was measured every hour, and cell cultures were diluted with YPD to maintain an OD_{660} between 0.85 and 1.3 (32).

RNA preparation

Total RNA was extracted using the hot phenol method. The collected cells were resuspended in 400 µL of AE buffer (50 mM sodium acetate (pH 5.0) and 10 mM EDTA) and 40 µL of 10% SDS, and briefly mixed at room temperature. Then, 500 µL of AE-buffer-equilibrated phenol (pre-warmed at 65°C) was immediately added, and the samples were vigorously mixed for 1 min. The samples were incubated at 65°C for 5 min and mixed for 5 s every 30 s. After the incubation, the samples were centrifugated, and 300 µL of the resulting supernatant was collected. Next, 400 µL of phenol: chloroform (1:1) and 100 µL of water were added, and the samples were vigorously mixed for 1 min. Three hundred microliters of the supernatant were collected, and 400 µL of chloroform:isoamyl alcohol (24:1) and 100 µL of water were added, and the samples were vigorously mixed for 1 min. After centrifugation, 300 µL of the resulting supernatant was collected, and total RNA was recovered by ethanol precipitation. For electrophoresis, the solution volume of rRNA to be loaded onto a denaturing agarose gel was normalized according to cell numbers (estimated by the OD_{660} value) to compare the amount of rRNA per cell. After electrophoresis, the gel was stained with SYBR Gold (Thermo Fisher Scientific) to visualize the RNA.

Quantification of RNA by real-time RT-PCR

Total RNA prepared by the hot-phenol method was purified by NucleoSpin RNA Clean-up kit (Takara Bio), and 100 ng of each RNA sample was reverse-transcribed with PrimeScript RT Master Mix (Perfect Real Time) (Takara Bio). qPCR was performed using the QuantiTect SYBR Green PCR Kit (QIAGEN). Quantified rRNA was normalized to the cell number (estimated using the OD_{660} value).

Western blotting

Proteins were prepared according to a previously described method (57). To detect GFP-Atg8p and Rpl25p-GFP, an anti-GFP polyclonal antibody (Medical & Biological Laboratories) and a rabbit horseradish-peroxidase-linked IgG whole antibody (Sigma-Aldrich) were used as the primary and secondary antibodies, respectively. An anti-DYKDDDDK tag, monoclonal antibody (FUJIFILM Wako Pure Chemical Corporation), anti-mouse IgG, and a sheep horseradish-peroxidase-linked whole antibody (GE Healthcare) were also used for the detection of C-terminally FLAG-tagged Rny1p.

ALP assay

ALP assay was performed according to a previously described method (58). Strain PhoΔ60 was constructed based on the BY4742 background. Protein concentrations were determined using the Bradford method. α-Naphthyl phosphate disodium salt (Sigma-Aldrich) was used as a substrate, and fluorescence was measured at emission and excitation wavelengths of 360 nm and 465 nm, respectively.

Fluorescence microscopic analysis

FM-4-64 Dye (Thermo Fisher Scientific) and GRG post stain in 10,000× (Biocraft) were used to stain the vacuoles and RNA accumulated in the vacuoles, respectively. An Olympus BX40 microscope with a fluorescence system (Olympus) and an FV1200 laser-scanning microscope (Olympus) were used for imaging.

Statistical analysis

Statistical analyses were performed using JASP software (59).

AlphaFold2 modeling and structural alignments

The structural models were predicted using the AlphaFold2 Colab web server (https://colab.research.google.com/github/sokrypton/ColabFold/blob/main/AlphaFold2.ipynb) (41, 60). The reliability of the model was estimated using the pLDDT score. Structural alignments were performed, and figures were constructed using PyMOL 2.5.0 (Schrodinger). The pLDDT score was mapped onto the structure using the PSICO plugin (https://github.com/YoshitakaMo/pymol-psico).

Phylogenetic analysis

Fifty-five amino acid sequences of proteins belonging to the RNase T2 superfamily listed in Swiss-Prot were obtained using a UniProt search. Homologous amino acid sequences were removed using CD-HIT (61). The amino acid sequence of *Irpex lacteux* RNase T2 (Irp3, GenBank ID: BAC00516.1) was added. A phylogenetic tree was constructed using the Graph Splitting method (44).

Supporting information
This article contains supporting information.

Acknowledgments
We acknowledge Dr. Hiroshi Takagi (Nara Institute of Science and Technology) for providing the strain that genetically expressed Rpl25p-GFP. We thank the National Bio-Resource Project (NBRP) of the MEXT/AMED, Japan, for providing plasmid pRS316[GFP-ATG8]. We also thank RIKEN BRC through the National BioResource Project of MEXT, Japan, for providing the plasmid pGMH20 (RDB01956).

Funding
This work was supported by the JSPS KAKENHI (grant numbers JP25450093, JP16K07657, and JP20K21266) to T.O. and by JST SPRING (grant number JPMJSP2108) to A.M.

Conflict of interest
The authors declare that they have no conflicts of interest with the contents of this article.

References

1. Harrow, J., Frankish, A., Gonzalez, J. M., Tapanari, E., Diekhans, M., Kokocinski, F., Aken, B. L., Barrell, D., Zadissa, A., Searle, S., Barnes, I., Bignell, A., Boychenko, V., Hunt, T., Kay, M., Mukherjee, G., Rajan, J., Despacio-Reyes, G., Saunders, G., Steward, C., Harte, R., Lin, M., Howald, C., Tanzer, A., Derrien, T., Chrast, J., Walters, N., Balasubramanian, S., Pei, B., Tress, M., Rodriguez, J. M., Ezkurdia, I., van Baren, J., Brent, M., Haussler, D., Kellis, M., Valencia, A., Reymond, A., Gerstein, M., Guigó, R., and Hubbard, T. J. (2012) GENCODE: the reference human genome annotation for The ENCODE Project. *Genome Res.* **22**, 1760–1774
2. Zhao, Y., Li, H., Fang, S., Kang, Y., Wu, W., Hao, Y., Li, Z., Bu, D., Sun, N., Zhang, M. Q., and Chen, R. (2016) NONCODE 2016: an informative and valuable data source of long non-coding RNAs. *Nucleic Acids Res.* **44**, D203-8
3. Napoli, C., Lemieux, C., and Jorgensen, R. (1990) Introduction of a Chimeric Chalcone Synthase Gene into Petunia Results in Reversible Co-Suppression of Homologous Genes in trans. *Plant Cell*. **2**, 279–289
4. Fire, A., Xu, S., Montgomery, M. K., Kostas, S. A., Driver, S. E., and Mello, C. C. (1998) Potent and specific genetic interference by double-stranded RNA in Caenorhabditis elegans. *Nature*. **391**, 806–811
5. Jinek, M., Chylinski, K., Fonfara, I., Hauer, M., Doudna, J. A., and Charpentier, E. (2012) A programmable dual-RNA-guided DNA endonuclease in adaptive bacterial immunity. *Science*. **337**, 816–821
6. Cong, L., Ran, F. A., Cox, D., Lin, S., Barretto, R., Habib, N., Hsu, P. D., Wu, X., Jiang, W., Marraffini, L. A., and Zhang, F. (2013) Multiplex genome engineering using CRISPR/Cas systems. *Science*. **339**, 819–823
7. Irie, M. (1999) Structure-function relationships of acid ribonucleases: lysosomal, vacuolar, and periplasmic enzymes. *Pharmacol. Ther.* **81**, 77–89
8. Acquati, F., Morelli, C., Cinquetti, R., Bianchi, M. G., Porrini, D., Varesco, L., Gismondi, V., Rocchetti, R., Talevi, S., Possati, L., Magnanini, C., Tibiletti, M. G., Bernasconi, B., Daidone, M. G., Shridhar, V., Smith, D. I., Negrini, M., Barbanti-Brodano, G., and Taramelli, R. (2001) Cloning and characterization of a senescence inducing and class II tumor suppressor gene in ovarian carcinoma at chromosome region 6q27. *Oncogene*. **20**, 980–988
9. Henneke, M., Diekmann, S., Ohlenbusch, A., Kaiser, J., Engelbrecht, V., Kohlschütter, A., Krätzner, R., Madruga-Garrido, M., Mayer, M., Opitz, L., Rodriguez, D., Rüschendorf, F., Schumacher, J., Thiele, H., Thoms, S., Steinfeld, R., Nürnberg, P., and Gärtner, J. (2009) RNASET2-deficient cystic leukoencephalopathy resembles congenital cytomegalovirus brain infection. *Nat. Genet.* **41**, 773–775
10. Quan, C., Ren, Y.-Q., Xiang, L.-H., Sun, L.-D., Xu, A.-E., Gao, X.-H., Chen, H.-D., Pu, X.-M., Wu, R.-N., Liang, C.-Z., Li, J.-B., Gao, T.-W., Zhang, J.-Z., Wang, X.-L., Wang, J., Yang, R.-Y., Liang, L., Yu, J.-B., Zuo, X.-B., Zhang, S.-Q., Zhang, S.-M., Chen, G., Zheng, X.-D., Li, P., Zhu, J., Li, Y.-W., Wei, X.-D., Hong, W.-S., Ye, Y., Zhang, Y., Wu, W.-S., Cheng, H., Dong, P.-L., Hu, D.-Y., Li, Y., Li, M., Zhang, X., Tang, H.-Y., Tang, X.-F., Xu, S.-X., He, S.-M., Lv, Y.-M., Shen, M., Jiang, H.-Q., Wang, Y., Li, K., Kang, X.-J., Liu, Y.-Q., Sun, L., Liu, Z.-F., Xie, S.-Q., Zhu, C.-Y., Xu, Q., Gao, J.-P., Hu, W.-L., Ni, C., Pan, T.-M., Li, Y., Yao, S., He, C.-F., Liu, Y.-S., Yu, Z.-Y., Yin, X.-Y., Zhang, F.-Y., Yang, S., Zhou, Y., and Zhang, X.-J. (2010) Genome-wide association study for vitiligo identifies susceptibility loci at 6q27 and the MHC. *Nat. Genet.* **42**, 614–618
11. Chen, X.-J., Gong, X.-H., Yan, N., Meng, S., Qin, Q., Jiang, Y.-F., Zheng, H.-Y., and Zhang, J.-A. (2015) RNASET2 tag SNP but not CCR6 polymorphisms is associated with autoimmune thyroid diseases in the Chinese Han population. *BMC Med. Genet.* **16**, 11
12. Gabrielsen, I. S. M., Amundsen, S. S., Helgeland, H., Flåm, S. T., Hatinoor, N., Holm, K., Viken, M. K., and Lie, B. A. (2016) Genetic risk variants for autoimmune diseases that influence gene expression in thymus. *Hum. Mol. Genet.* **25**, 3117–3124
13. Ostendorf, T., Zillinger, T., Andryka, K., Schlee-Guimaraes, T. M., Schmitz, S., Marx, S.,

Bayrak, K., Linke, R., Salgert, S., Wegner, J., Grasser, T., Bauersachs, S., Soltesz, L., Hübner, M. P., Nastaly, M., Coch, C., Kettwig, M., Roehl, I., Henneke, M., Hoerauf, A., Barchet, W., Gärtner, J., Schlee, M., Hartmann, G., and Bartok, E. (2020) Immune Sensing of Synthetic, Bacterial, and Protozoan RNA by Toll-like Receptor 8 Requires Coordinated Processing by RNase T2 and RNase 2. *Immunity*. **52**, 591-605.e6

14. Greulich, W., Wagner, M., Gaidt, M. M., Stafford, C., Cheng, Y., Linder, A., Carell, T., and Hornung, V. (2019) TLR8 Is a Sensor of RNase T2 Degradation Products. *Cell*. **179**, 1264-1275.e13
15. Liu, K., Sato, R., Shibata, T., Hiranuma, R., Reuter, T., Fukui, R., Zhang, Y., Ichinohe, T., Ozawa, M., Yoshida, N., Latz, E., and Miyake, K. (2021) Skewed endosomal RNA responses from TLR7 to TLR3 in RNase T2-deficient macrophages. *Int. Immunol.* **33**, 479–490
16. Miyake, K., Shibata, T., Fukui, R., Sato, R., Saitoh, S.-I., and Murakami, Y. (2022) Nucleic Acid Sensing by Toll-Like Receptors in the Endosomal Compartment. *Front. Immunol.* **13**, 941931
17. Löffler, A., Abel, S., Jost, W., Beintema, J. J., and Glund, K. (1992) Phosphate-Regulated Induction of Intracellular Ribonucleases in Cultured Tomato (Lycopersicon esculentum) Cells. *Plant Physiol.* **98**, 1472–1478
18. Taylor, C. B., Bariola, P. A., delCardayré, S. B., Raines, R. T., and Green, P. J. (1993) RNS2: a senescence-associated RNase of Arabidopsis that diverged from the S-RNases before speciation. *Proc. Natl. Acad. Sci. U. S. A.* **90**, 5118–5122
19. Bariola, P. A., Howard, C. J., Taylor, C. B., Verburg, M. T., Jaglan, V. D., and Green, P. J. (1994) The Arabidopsis ribonuclease gene RNS1 is tightly controlled in response to phosphate limitation. *Plant J.* **6**, 673–685
20. Takayama, S., and Isogai, A. (2005) Self-incompatibility in plants. *Annu. Rev. Plant Biol.* **56**, 467–489
21. Hua, Z.-H., Fields, A., and Kao, T.-H. (2008) Biochemical models for S-RNase-based self-incompatibility. *Mol. Plant*. **1**, 575–585
22. Schneider, R., Unger, G., Stark, R., Schneider-Scherzer, E., and Thiel, H.-J. (1993) Identification of a Structural Glycoprotein of an RNA Virus as a Ribonuclease. *Science*. **261**, 1169–1171
23. Langedijk, J. P. M. (2002) Translocation activity of C-terminal domain of pestivirus Erns and ribotoxin L3 loop. *J. Biol. Chem.* **277**, 5308–5314
24. Makarov, A. A., and Ilinskaya, O. N. (2003) Cytotoxic ribonucleases: molecular weapons and their targets. *FEBS Lett.* **540**, 15–20
25. Fontaine, B. M., Martin, K. S., Garcia-Rodriguez, J. M., Jung, C., Briggs, L., Southwell, J. E., Jia, X., and Weinert, E. E. (2018) RNase I regulates Escherichia coli 2',3'-cyclic nucleotide monophosphate levels and biofilm formation. *Biochem. J.* **475**, 1491–1506
26. MacIntosh, G. C., Bariola, P. A., Newbigin, E., and Green, P. J. (2001) Characterization of Rny1, the Saccharomyces cerevisiae member of the T2 RNase family of RNases: unexpected functions for ancient enzymes? *Proc. Natl. Acad. Sci. U. S. A.* **98**, 1018–1023
27. Shcherbik, N. (2013) Golgi-mediated glycosylation determines residency of the T2 RNase Rny1p in Saccharomyces cerevisiae. *Traffic*. **14**, 1209–1227
28. Kitahara, K., and Miyazaki, K. (2011) Specific inhibition of bacterial RNase T2 by helix 41 of 16S ribosomal RNA. *Nat. Commun.* **2**, 549
29. Haud, N., Kara, F., Diekmann, S., Henneke, M., Willer, J. R., Hillwig, M. S., Gregg, R. G., Macintosh, G. C., Gärtner, J., Alia, A., and Hurlstone, A. F. L. (2011) rnaset2 mutant zebrafish model familial cystic leukoencephalopathy and reveal a role for RNase T2 in degrading ribosomal RNA. *Proc. Natl. Acad. Sci. U. S. A.* **108**, 1099–1103
30. Hillwig, M. S., Contento, A. L., Meyer, A., Ebany, D., Bassham, D. C., and Macintosh, G. C. (2011) RNS2, a conserved member of the RNase T2 family, is necessary for ribosomal RNA decay in plants. *Proc. Natl. Acad. Sci. U. S. A.* **108**, 1093–1098
31. Andersen, K. L., and Collins, K. (2012) Several RNase T2 enzymes function in induced tRNA and rRNA turnover in the ciliate Tetrahymena. *Mol. Biol. Cell*. **23**, 36–44
32. Pestov, D. G., and Shcherbik, N. (2012) Rapid cytoplasmic turnover of yeast ribosomes in

response to rapamycin inhibition of TOR. *Mol. Cell. Biol.* **32**, 2135–2144
33. Huang, H., Kawamata, T., Horie, T., Tsugawa, H., Nakayama, Y., Ohsumi, Y., and Fukusaki, E. (2015) Bulk RNA degradation by nitrogen starvation-induced autophagy in yeast. *EMBO J.* **34**, 154–168
34. Kraft, C., Deplazes, A., Sohrmann, M., and Peter, M. (2008) Mature ribosomes are selectively degraded upon starvation by an autophagy pathway requiring the Ubp3p/Bre5p ubiquitin protease. *Nat. Cell Biol.* **10**, 602–610
35. Powers, T., and Walter, P. (1999) Regulation of ribosome biogenesis by the rapamycin-sensitive TOR-signaling pathway in Saccharomyces cerevisiae. *Mol. Biol. Cell*. **10**, 987–1000
36. Floyd, B. E., Morriss, S. C., MacIntosh, G. C., and Bassham, D. C. (2015) Evidence for autophagy-dependent pathways of rRNA turnover in Arabidopsis. *Autophagy*. **11**, 2199–2212
37. Wyant, G. A., Abu-Remaileh, M., Frenkel, E. M., Laqtom, N. N., Dharamdasani, V., Lewis, C. A., Chan, S. H., Heinze, I., Ori, A., and Sabatini, D. M. (2018) NUFIP1 is a ribosome receptor for starvation-induced ribophagy. *Science*. **360**, 751–758
38. McKeegan, K. S., Debieux, C. M., Boulon, S., Bertrand, E., and Watkins, N. J. (2007) A dynamic scaffold of pre-snoRNP factors facilitates human box C/D snoRNP assembly. *Mol. Cell. Biol.* **27**, 6782–6793
39. Boulon, S., Marmier-Gourrier, N., Pradet-Balade, B., Wurth, L., Verheggen, C., Jády, B. E., Rothé, B., Pescia, C., Robert, M.-C., Kiss, T., Bardoni, B., Krol, A., Branlant, C., Allmang, C., Bertrand, E., and Charpentier, B. (2008) The Hsp90 chaperone controls the biogenesis of L7Ae RNPs through conserved machinery. *J. Cell Biol.* **180**, 579–595
40. Quinternet, M., Rothé, B., Barbier, M., Bobo, C., Saliou, J.-M., Jacquemin, C., Back, R., Chagot, M.-E., Cianférani, S., Meyer, P., Branlant, C., Charpentier, B., and Manival, X. (2015) Structure/Function Analysis of Protein–Protein Interactions Developed by the Yeast Pih1 Platform Protein and Its Partners in Box C/D snoRNP Assembly. *J. Mol. Biol.* **427**, 2816–2839
41. Jumper, J., Evans, R., Pritzel, A., Green, T., Figurnov, M., Ronneberger, O., Tunyasuvunakool, K., Bates, R., Žídek, A., Potapenko, A., Bridgland, A., Meyer, C., Kohl, S. A. A., Ballard, A. J., Cowie, A., Romera-Paredes, B., Nikolov, S., Jain, R., Adler, J., Back, T., Petersen, S., Reiman, D., Clancy, E., Zielinski, M., Steinegger, M., Pacholska, M., Berghammer, T., Bodenstein, S., Silver, D., Vinyals, O., Senior, A. W., Kavukcuoglu, K., Kohli, P., and Hassabis, D. (2021) Highly accurate protein structure prediction with AlphaFold. *Nature*. **596**, 583–589
42. Holm, L. (2020) DALI and the persistence of protein shape. *Protein Sci.* **29**, 128–140
43. Sagane, Y., Hayashi, S., Akiyama, T., and Matsumoto, T. (2016) Conformational divergence in the HA-33/HA-17 trimer of serotype C and D botulinum toxin complex. *Biochemical and*
44. Matsui, M., and Iwasaki, W. (2020) Graph Splitting: A Graph-Based Approach for Superfamily-Scale Phylogenetic Tree Reconstruction. *Syst. Biol.* **69**, 265–279
45. Kobayashi, H., Itagaki, T., Inokuchi, N., Ohgi, K., Wada, T., Iwama, M., and Irie, M. (2003) A new type of RNase T2 ribonuclease in two Basidiomycetes fungi, Lentinus edodes and Irpex lacteus. *Biosci. Biotechnol. Biochem.* **67**, 2307–2310
46. Hulst, M. M., Himes, G., Newbigin, E., and Moormann, R. J. (1994) Glycoprotein E2 of classical swine fever virus: expression in insect cells and identification as a ribonuclease. *Virology*. **200**, 558–565
47. Luhtala, N., and Parker, R. (2010) T2 Family ribonucleases: ancient enzymes with diverse roles. *Trends Biochem. Sci.* **35**, 253–259
48. Floyd, B. E., Mugume, Y., Morriss, S. C., MacIntosh, G. C., and Bassham, D. C. (2017) Localization of RNS2 ribonuclease to the vacuole is required for its role in cellular homeostasis. *Planta*. **245**, 779–792
49. Liu, Y., Zou, W., Yang, P., Wang, L., Ma, Y., Zhang, H., and Wang, X. (2018) Autophagy-dependent ribosomal RNA degradation is essential for maintaining nucleotide homeostasis during C. elegans development. *Elife*. 10.7554/eLife.36588
50. Ossareh-Nazari, B., Bonizec, M., Cohen, M., Dokudovskaya, S., Delalande, F., Schaeffer, C., Van Dorsselaer, A., and Dargemont, C. (2010) Cdc48 and Ufd3, new partners of the ubiquitin

protease Ubp3, are required for ribophagy. *EMBO Rep.* **11**, 548–554
51. Bardoni, B., Willemsen, R., Weiler, I. J., Schenck, A., Severijnen, L.-A., Hindelang, C., Lalli, E., and Mandel, J.-L. (2003) NUFIP1 (nuclear FMRP interacting protein 1) is a nucleocytoplasmic shuttling protein associated with active synaptoneurosomes. *Exp. Cell Res.* **289**, 95–107
52. Rothé, B., Saliou, J.-M., Quinternet, M., Back, R., Tiotiu, D., Jacquemin, C., Loegler, C., Schlotter, F., Peña, V., Eckert, K., Moréra, S., Van Dorsselaer, A., Branlant, C., Massenet, S., Sanglier-Cianférani, S., Manival, X., and Charpentier, B. (2014) Protein Hit1, a novel box C/D snoRNP assembly factor, controls cellular concentration of the scaffolding protein Rsa1 by direct interaction. *Nucleic Acids Res.* **42**, 10731–10747
53. Nürnberger, T., Abel, S., Jost, W., and Glund, K. (1990) Induction of an Extracellular Ribonuclease in Cultured Tomato Cells upon Phosphate Starvation. *Plant Physiol.* **92**, 970–976
54. Levin, D. E. (2011) Regulation of cell wall biogenesis in Saccharomyces cerevisiae: the cell wall integrity signaling pathway. *Genetics*. **189**, 1145–1175
55. Khvorova, A., Kwak, Y. G., Tamkun, M., Majerfeld, I., and Yarus, M. (1999) RNAs that bind and change the permeability of phospholipid membranes. *Proc. Natl. Acad. Sci. U. S. A.* **96**, 10649–10654
56. Tatehashi, Y., Watanabe, D., and Takagi, H. (2016) γ-Glutamyl kinase is involved in selective autophagy of ribosomes in Saccharomyces cerevisiae. *FEBS Lett.* **590**, 2906–2914
57. Zhang, T., Lei, J., Yang, H., Xu, K., Wang, R., and Zhang, Z. (2011) An improved method for whole protein extraction from yeast Saccharomyces cerevisiae. *Yeast*. **28**, 795–798
58. Noda, T., and Klionsky, D. J. (2008) The quantitative Pho8Delta60 assay of nonspecific autophagy. *Methods Enzymol.* **451**, 33–42
59. Love, J., Selker, R., Marsman, M., Jamil, T., Dropmann, D., Verhagen, J., Ly, A., Gronau, Q. F., Šmíra, M., Epskamp, S., Matzke, D., Wild, A., Knight, P., Rouder, J. N., Morey, R. D., and Wagenmakers, E.-J. (2019) JASP: Graphical Statistical Software for Common Statistical Designs. *J. Stat. Softw.* **88**, 1–17
60. Mirdita, M., Schütze, K., Moriwaki, Y., Heo, L., Ovchinnikov, S., and Steinegger, M. (2022) ColabFold: making protein folding accessible to all. *Nat. Methods*. **19**, 679–682
61. Li, W., and Godzik, A. (2006) Cd-hit: a fast program for clustering and comparing large sets of protein or nucleotide sequences. *Bioinformatics*. **22**, 1658–1659

Footnotes

GFP, green fluorescent protein
NBRP, National Bio-Resource Project
NUFIP1, nuclear fragile X mental retardation–interacting protein 1
OD660, optical density at 660 nm
qRT-PCR, quantitative RT-PCR
SD synthetic dextrose
SG synthetic galactose
snoRNP, small nucleolar ribonucleoprotein
YPD, 1% yeast extract, 2% polypeptone, 2% glucose

Figure 1

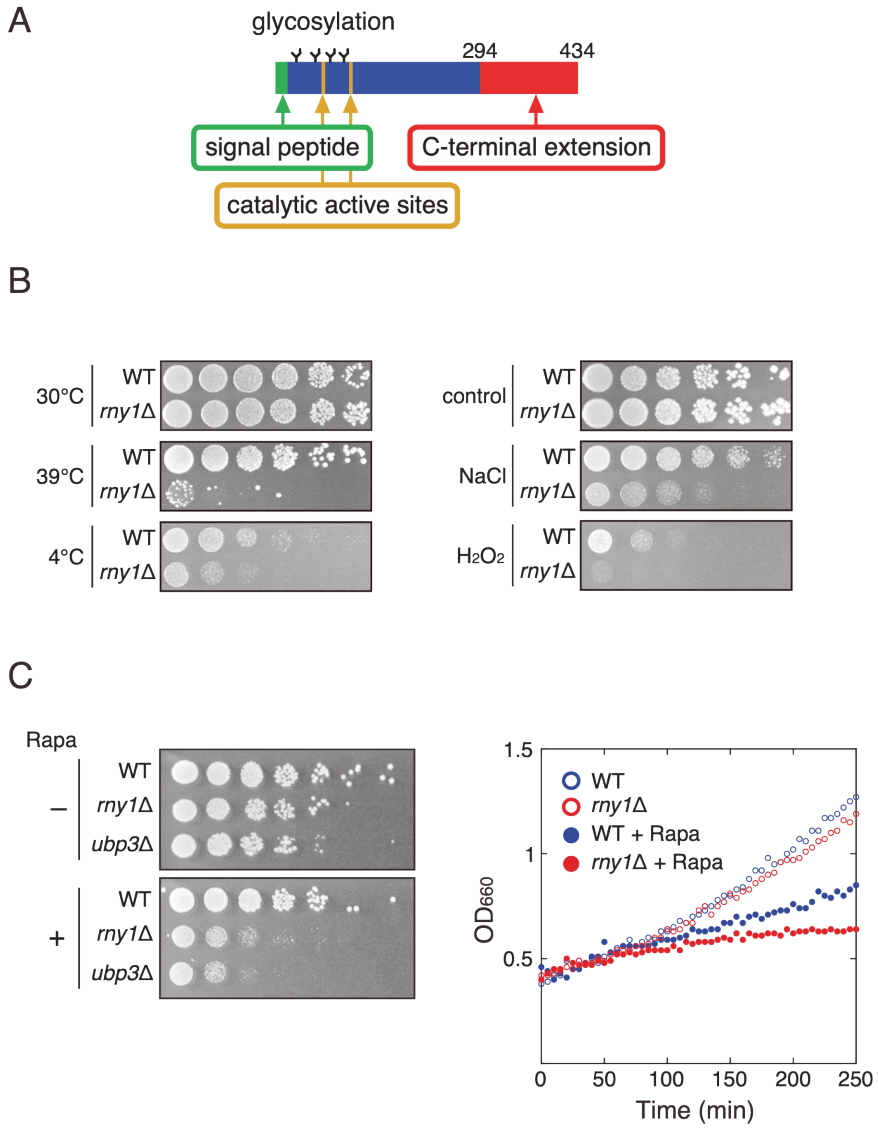

Figure 1 Rny1p responses to various stress conditions.
A, Schematic structure of Rny1p is shown. Rny1p possesses signal peptides and C-terminal extensions at the N- and C-termini, respectively. The glycosylation and catalytic active sites, CASI and CASII, and amino acid numbers at the N-terminus are indicated. CASI and CASII contain catalytic residues His87 and His160, respectively. *B (left panel)*, wild-type and *rny1*Δ strains were cultivated in YPD medium to reach an optical density at 660 nm (OD_{660}) of 0.3 to 0.4. They were then serially diluted five times, spotted onto plates, and cultivated at the indicated temperatures. To examine the sensitivity to cold shock, the plate was incubated at 4°C, and the cultivation temperature was then shifted to 30°C to obtain visible colonies (see Experimental procedures). *B (right panel),* Diluted cultures of the wild-type and *rny1*Δ strains were spotted onto a YPD medium containing NaCl (50 g/L) or H_2O_2 (0.3 mM). *C (left panel)*, the cells were cultured and diluted as shown in (*B*) and spotted onto YPD plates with or without rapamycin (5 nM). Strain *ubp3*Δ, reported to be sensitive to rapamycin, was used as a control (34). *C (right panel),* Wild-type and *rny1*Δ strains grown in YPD. When the OD_{660} reached 0.4, rapamycin (100 nM) was added, and the OD_{660} was monitored over time. Open blue and red circles indicate the OD curves of the wild-type and *rny1*Δ strains, while solid blue and red circles indicate those grown in the presence of rapamycin, respectively.

Figure 2

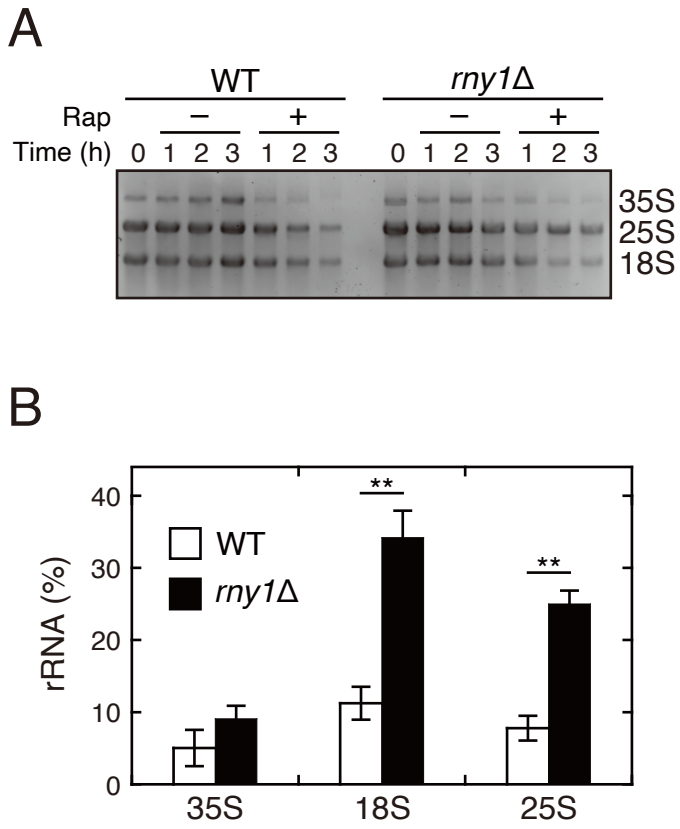

Figure 2 Rny1p degrades 18S and 25S rRNA in response to rapamycin treatment. *A*, Wild-type and *rny1*Δ strains were cultivated at 30°C until the OD_{660} reached 0.5. Rapamycin (100 nM) was then added, and cultivation was continued. Cells were collected at the indicated time points, and total RNA was extracted. After preparation, the amount of total RNA was normalized to the cell number and loaded onto a denaturing agarose gel. *B*, Cells were cultivated as shown in (*A*), and when the OD_{660} reached 0.4, rapamycin (100 nM) was added, and the cells were further incubated for 3 h. Total RNA was prepared, and 18S, 25S, and 35S rRNA were quantified by quantitative RT-PCR (qRT-PCR) analysis. The amount of rRNA remaining after rapamycin treatment was calculated as follows: rRNA (%) = 100 × (amount of RNA prepared from rapamycin-treated cells)/(amount of RNA prepared from cells before rapamycin treatment). Data are presented as the means ± standard error of 3 independent experiments. Asterisks indicate significant differences ($^{**}P < 0.01$, Student's t-test).

Figure 3

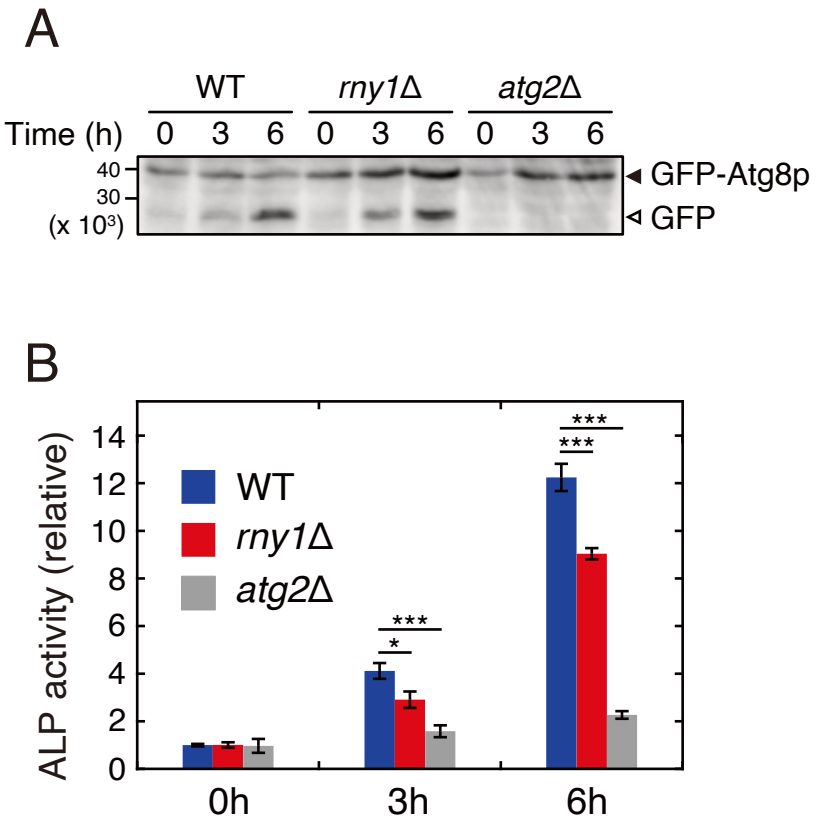

Figure 3 Autophagic activity is decreased in the *rny1*Δ strain.
A, Wild-type, *rny1*Δ, and *atg2*Δ strains expressing GFP-Atg8p were grown in SD medium until the OD_{660} reached 0.4. The cells were then washed, suspended in nitrogen-depleted SD medium (SD (-N) medium), and cultured. Cells were collected at the indicated time points. Cell lysates were prepared and electrophoresed, and western blotting was performed using an anti-GFP antibody. Solid and open arrowheads indicate GFP-Atg8p and cleaved GFP fragments, respectively. *B*, Wild-type, *rny1*Δ, and *atg2*Δ strains expressing the cytosolic form of Pho8p (Pho8Δ60) were cultured in SD (-N) medium, and cell lysates were prepared at the indicated time points. Phosphatase activity was quantified to evaluate the autophagic activity (ALP assay). Data are presented as the means ± standard error of 6 independent experiments. Asterisks indicate significant differences (*$P < 0.05$, ***$P < 0.001$, Student's t-test).

Figure 4

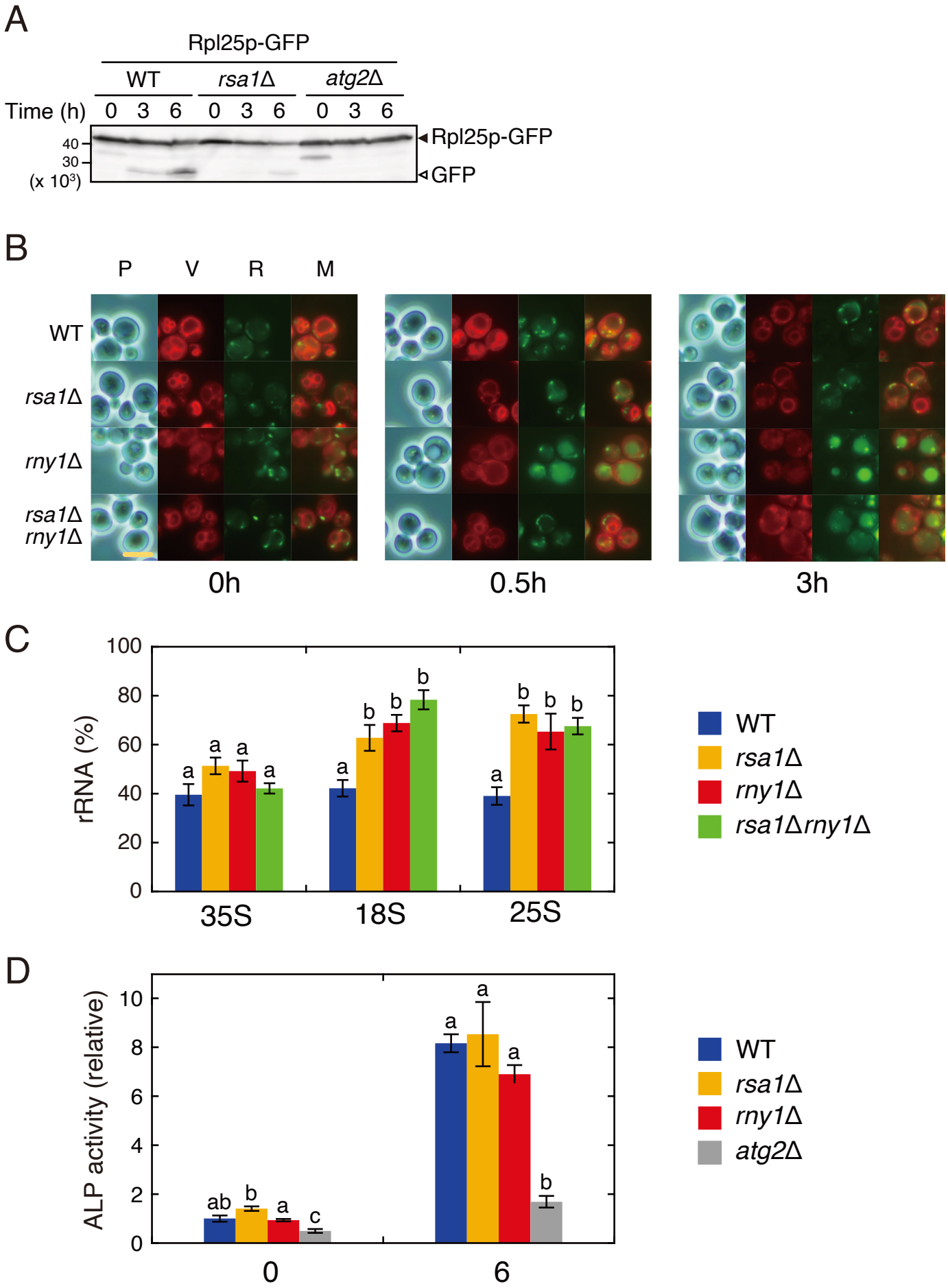
A
Rpl25p-GFP
WT
rsa1Δ
atg2Δ
Time (h)
0 3 6 0 3 6 0 3 6
40
30
(x 10³)
Rpl25p-GFP
GFP
B
P V R M
WT
rsa1Δ
rny1Δ
rsa1Δ rny1Δ
0h
0.5h
3h
C
rRNA (%)
100
80
60
40
20
0
35S
18S
25S
WT
rsa1Δ
rny1Δ
rsa1Δrny1Δ
D
ALP activity (relative)
10
8
6
4
2
0
0
6
WT
rsa1Δ
rny1Δ
atg2Δ

Figure 4 (continued)

Figure 4 Degradation of ribosomes induced by nitrogen starvation depends on Rsa1p. *A*, Wild-type, *rsa1*Δ, and *atg2*Δ strains expressing the GFP-tagged ribosomal protein (Rpl25p-GFP) were cultured to an OD_{660} of 0.4. Then nitrogen starvation was induced, and cell lysates were prepared at the indicated time points. Western blotting was performed using an anti-GFP antibody, and Rpl25p degradation was evaluated. *B*, Wild-type cells and cells lacking Rsa1p, Rny1p, or both of Rsa1p and Rny1p were grown under nitrogen starvation conditions, and vacuoles and RNA were stained at the indicated time points. "P" labeled above the panels indicates the observation was made by phase-constant microscopy, while "V" and "R" indicate the observation of cells in which vacuoles or RNA were stained, respectively. "M" indicates a merged panel with "V" and "R." Scale bar represents 5 µm. *C*, Wild-type, *rsa1*Δ, *rny1*Δ, and *rsa1*Δ*rny1*Δ strains were grown in SD or SD (-N) medium. After 3 h of cultivation, total RNA was prepared and reverse-transcribed, and qRT-PCR analysis was performed, as shown in Fig. 2B, to quantify 35S, 25S, and 18S rRNA. The amount of rRNA remaining after induction of nitrogen starvation was calculated as follows: rRNA (%) = 100 × (amount of RNA prepared from cells cultured in SD (-N) medium)/(amount of RNA prepared from cells cultured in SD medium). *D*, Nitrogen starvation was induced in wild-type, *rsa1*Δ, *rny1*Δ, and *rsa1*Δ*rny1*Δ strains expressing Pho8Δ60 for 3 h, and then ALP assays were performed. Data are presented as means ± standard error from 4 and 3 independent experiments in (*C*) and (*D*), respectively. Statistical analyses were conducted for 35S, 18S, and 25S rRNA in (*C*) and at each time point in (*D*). Different letters indicate significant differences ($P < 0.05$, Tukey-Kramer test).

Figure 5

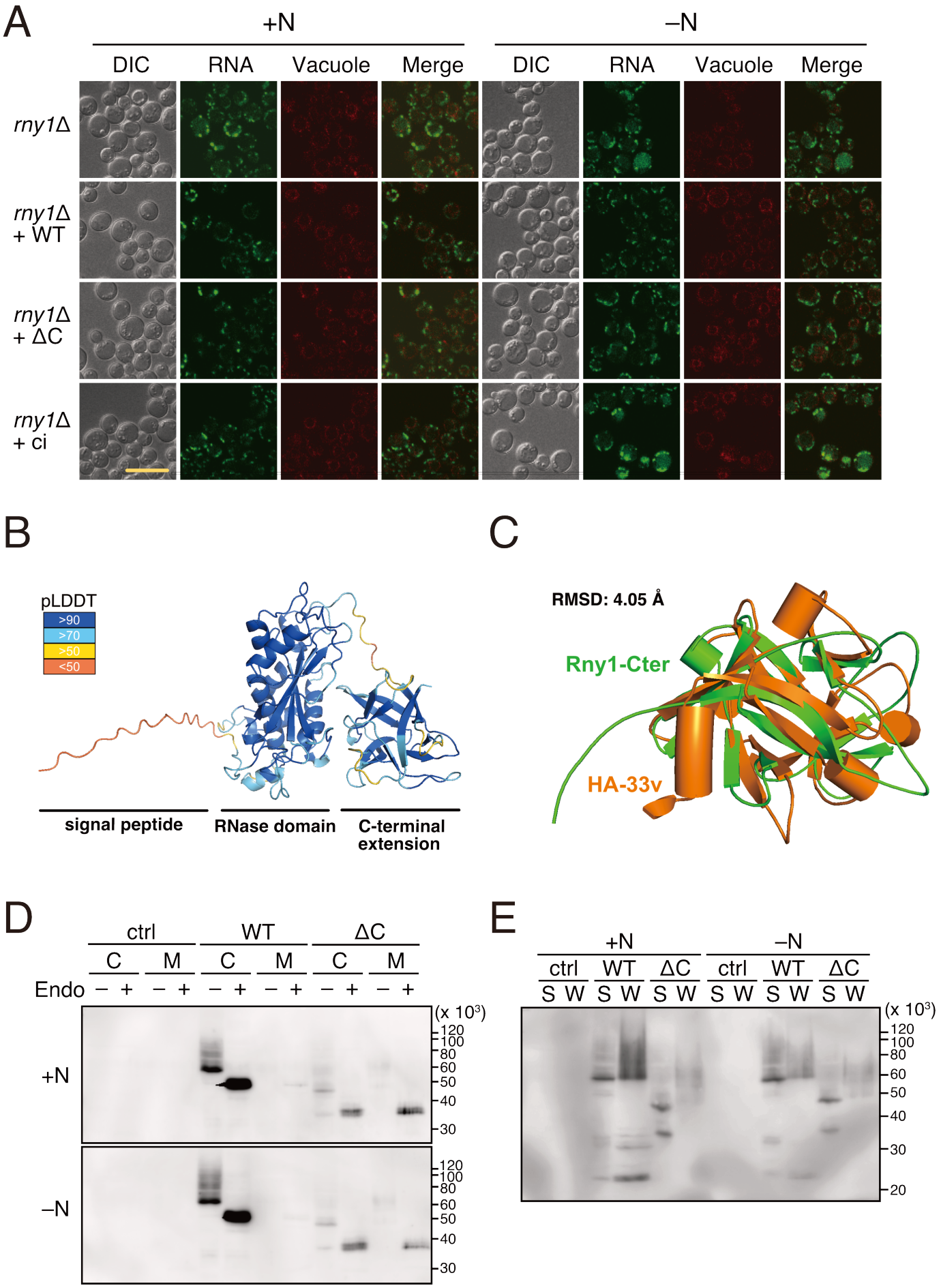
A
+N
–N
DIC
RNA
Vacuole
Merge
rny1Δ
rny1Δ + WT
rny1Δ + ΔC
rny1Δ + ci
B
pLDDT
>90
>70
>50
<50
signal peptide
RNase domain
C-terminal extension
C
RMSD: 4.05 Å
Rny1-Cter
HA-33v
D
ctrl
WT
ΔC
C
M
Endo
+N
–N
(x 10³)
120
100
80
60
50
40
30
E
+N
–N
ctrl
WT
ΔC
S
W
(x 10³)
120
100
80
60
50
40
30
20

Figure 5 (continued)

Figure 5 Rny1p binds to the cell wall *via* the C-terminal extension, which is not required for RNA degradation in the vacuole.
A, Strains expressing Rny1p-F, Rny1pΔC-F, or Rny1p(H87F/H160F)-F from the chromosomes were cultured in SD or SD (-N) medium for 3 h. After staining the vacuoles with RNA, fluorescence confocal microscopic analysis was performed. The scale bar represents 10 μm. *B*, The structure of Rny1p was predicted using AlphaFold2 with confidence levels mapped onto the structure. The signal peptide, RNase domain, and C-terminal extension are indicated. *C,* Structural alignment of the C-terminal extension of predicted Rny1p (labeled Rny1-Cter) with the crystal structure of the variable region of HA-33 (PDB ID:5B2H, labeled HA-33v). *D*, Wild-type strain expressing Rny1p-F or Rny1pΔC-F from a plasmid was cultivated in SG medium until the OD_{660} reached 0.3. These cells were washed, suspended in SG or SG (-N) medium, and cultured for another 3 h. After cultivation, the cells were collected, cell lysates were prepared, and the culture medium was concentrated 200 times by ultrafiltration. These samples were then electrophoresed, and western blotting was performed using an anti-FLAG antibody. "C" and "M" indicate that cell lysate or concentrated medium was loaded, respectively, while "Endo" indicates endoglycosidase H treatment. The exposure time of the lower panel was longer than that of the upper panel because of the lower signal intensity of the lower panel. *E*, Cells were cultured as described in (*D*) for 3 h, harvested, and treated with zymolyase. After centrifugation, spheroplasts were collected, and cell lysates were prepared. The final volume of the cell lysate and supernatant containing the zymolyase-treated cell wall fraction was 500 μL and 100 μL, respectively. An equal volume of samples was loaded onto a gel, and SDS-PAGE was carried out, followed by western blotting as shown in (*D*). "S" and "W" indicate that the cell lysates were prepared from spheroplasts or cell wall fractions, respectively. In (*D*) and (*E*), "ctrl," "WT," and "ΔC" indicate that samples were prepared from strains harboring pGMH20 (empty vector), pGMH20-*RNY1-F,* and pGMH20-*RNY1*ΔC-*F*, respectively.

Figure 6

A

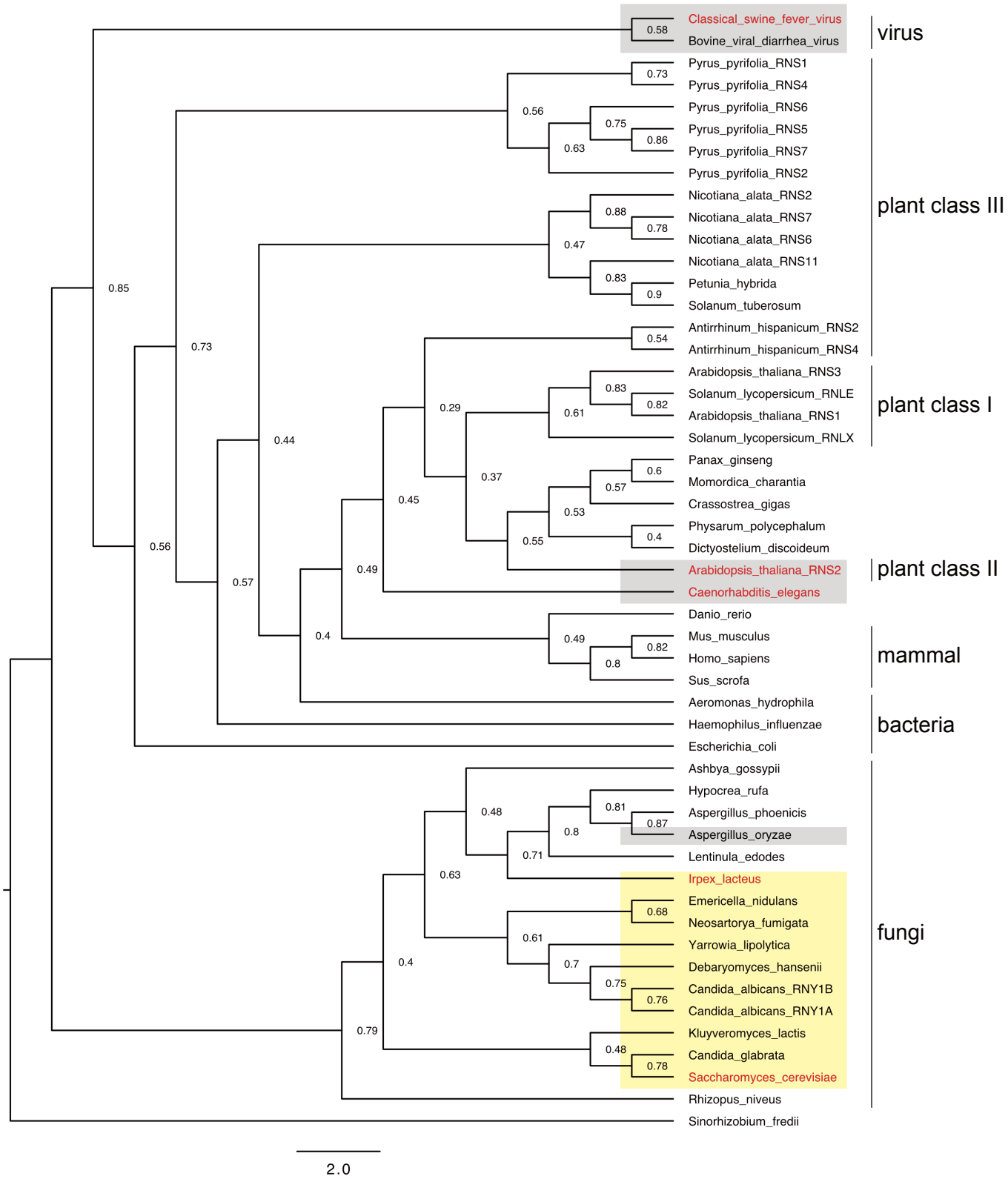
Classical_swine_fever_virus
Bovine_viral_diarrhea_virus
virus
Pyrus_pyrifolia_RNS1
Pyrus_pyrifolia_RNS4
Pyrus_pyrifolia_RNS6
Pyrus_pyrifolia_RNS5
Pyrus_pyrifolia_RNS7
Pyrus_pyrifolia_RNS2
Nicotiana_alata_RNS2
Nicotiana_alata_RNS7
Nicotiana_alata_RNS6
Nicotiana_alata_RNS11
Petunia_hybrida
Solanum_tuberosum
Antirrhinum_hispanicum_RNS2
Antirrhinum_hispanicum_RNS4
plant class III
Arabidopsis_thaliana_RNS3
Solanum_lycopersicum_RNLE
Arabidopsis_thaliana_RNS1
Solanum_lycopersicum_RNLX
plant class I
Panax_ginseng
Momordica_charantia
Crassostrea_gigas
Physarum_polycephalum
Dictyostelium_discoideum
Arabidopsis_thaliana_RNS2
Caenorhabditis_elegans
plant class II
Danio_rerio
Mus_musculus
Homo_sapiens
Sus_scrofa
mammal
Aeromonas_hydrophila
Haemophilus_influenzae
Escherichia_coli
bacteria
Ashbya_gossypii
Hypocrea_rufa
Aspergillus_phoenicis
Aspergillus_oryzae
Lentinula_edodes
Irpex_lacteus
Emericella_nidulans
Neosartorya_fumigata
Yarrowia_lipolytica
Debaryomyces_hansenii
Candida_albicans_RNY1B
Candida_albicans_RNY1A
Kluyveromyces_lactis
Candida_glabrata
Saccharomyces_cerevisiae
Rhizopus_niveus
Sinorhizobium_fredii
fungi
2.0

Figure 6 (continued)

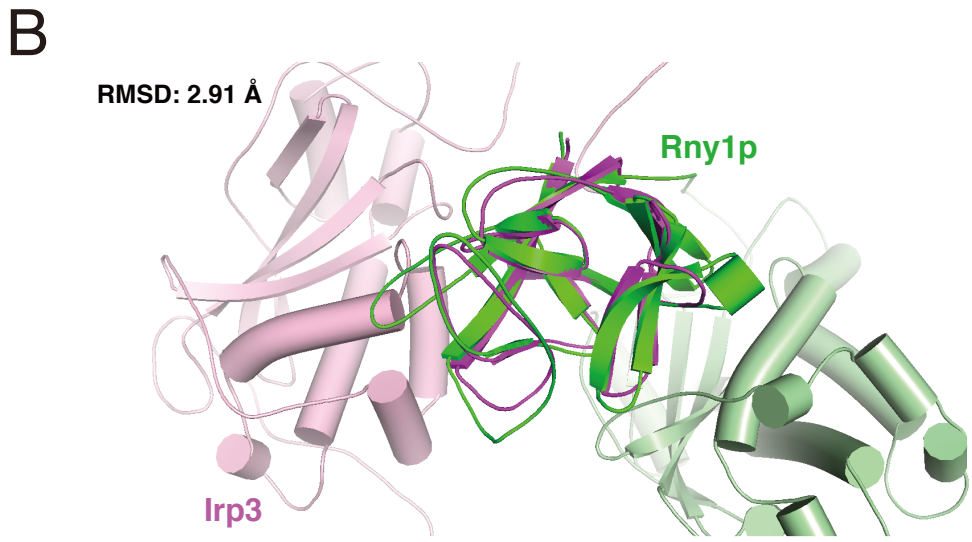

Figure 6. Diversity of the C-terminal extension among the RNase T2 superfamily.
A, A phylogenetic tree of the RNase T2 superfamily was created based on amino acid sequences. Organisms possessing C-terminal extensions homologous to Rny1p are shaded yellow, whereas those not homologous to Rny1p are shaded grey. RNase T2 of classical swine fever virus, *Arabidopsis thaliana*, *Caenorhabditis elegans*, *Irpex lacteus*, and *S. cerevisiae* are discussed in this paper, and their genus names are colored in red. *B*, Structural alignment of the C-terminal extension of Rny1p (labeled Rny1p) was performed with the predicted *Irpex lacteux* RNase T2 (labeled Irp3).

Table 1

Yeast strains used in this study

Strain	Genotype	Source
BY4741	*MAT*a *his3Δ1 leu2Δ0 met15Δ0 ura3Δ0*	Euroscarf
BY4742	*MAT*α *his3Δ1 leu2Δ0 lys2Δ0 ura3Δ0*	Euroscarf
Y12129	*MAT*α *his3Δ1 leu2Δ0 lys2Δ0 ura3Δ0 rny1Δ::kanMX4*	Euroscarf
Y16148	*MAT*α *his3Δ1 leu2Δ0 lys2Δ0 ura3Δ0 ubp3Δ::kanMX4*	Euroscarf
Y11099	*MAT*α *his3Δ1 leu2Δ0 lys2Δ0 ura3Δ0 rsa1Δ::kanMX4*	Euroscarf
Y11970	*MAT*α *his3Δ1 leu2Δ0 lys2Δ0 ura3Δ0 atg2Δ::kanMX4*	Euroscarf
rny1Δrsa1Δ	*MAT*α *his3Δ1 leu2Δ0 lys2Δ0 ura3Δ0 rsa1Δ::kanMX4 rny1Δ::URA3*	This study
pho8Δ60	*MAT*α *his3Δ1 leu2Δ0 lys2Δ0 ura3Δ0 pho8Δ60::clonNAT*	This study
pho8Δ60rny1Δ	*MAT*α *his3Δ1 leu2Δ0 lys2Δ0 ura3Δ0 pho8Δ60::clonNAT rny1Δ::kanMX4*	This study
pho8Δ60rsa1Δ	*MAT*α *his3Δ1 leu2Δ0 lys2Δ0 ura3Δ0 pho8Δ60::clonNAT rsa1Δ::kanMX4*	This study
pho8Δ60atg2Δ	*MAT*α *his3Δ1 leu2Δ0 lys2Δ0 ura3Δ0 pho8Δ60::clonNAT atg2Δ::kanMX4*	This study
RNY1-null	*MAT*α *his3Δ1 leu2Δ0 lys2Δ0 ura3Δ0 rny1Δ::URA3*	This study
RNY1-F_int	*MAT*α *his3Δ1 leu2Δ0 lys2Δ0 ura3Δ0 rny1Δ::RNY1-F::URA3*	This study
RNY1ΔC-F_int	*MAT*α *his3Δ1 leu2Δ0 lys2Δ0 ura3Δ0 rny1Δ::RNY1ΔC-F::URA3*	This study
RNY1ci-F_int	*MAT*α *his3Δ1 leu2Δ0 lys2Δ0 ura3Δ0 rny1Δ::RNY1(H87F/H160F)-F::URA3*	This study
RPL25-GFP	*MAT*a *his3Δ1 leu2Δ0 met15Δ0 ura3Δ0 rpl25Δ::RPL25-GFP-hph*	ref. 56
RPL25-GFPrsa1Δ	*MAT*a *his3Δ1 leu2Δ0 met15Δ0 ura3Δ0 rpl25Δ::RPL25-GFP-hph rsa1Δ::kanMX4*	This study
RPL25-GFPatg2Δ	*MAT*a *his3Δ1 leu2Δ0 met15Δ0 ura3Δ0 rpl25Δ::RPL25-GFP-hph atg2Δ::kanMX4*	This study